LIMNOLOGY and OCEANOGRAPHY

ASLO

Limnol. Oceanogr. 9999, 2021, 1–19

doi: 10.1002/lno.11762

Connectivity of coastal and neritic fish larvae to the deep waters

Jesus C. Compaire [1,3] **Paula Pérez-Brunius** [1] **Sylvia Patricia Adelheid Jiménez-Rosenberg** [2] **Javier Rodríguez Outerelo** [1] **Laura del Pilar Echeverri García** [1] **Sharon Z. Herzka** [1*]

[1]Centro de Investigación Científica y de Educación Superior de Ensenada (CICESE), Ensenada, Baja California, Mexico
[2]Instituto Politécnico Nacional-Centro Interdisciplinario de Ciencias Marinas (IPN-CICIMAR), La Paz, Baja California Sur, Mexico
[3]Present address: CONICET – Universidad de Buenos Aires, Centro de Investigaciones del Mar y la Atmósfera (CIMA), Buenos Aires, Argentina

Abstract

Four ichthyoplankton cruises and backward tracking experiments were conducted to study the connectivity of coastal and neritic fish larvae over the continental slope and to the oceanic deep-water region of the western Gulf of Mexico. Distribution patterns of larval abundance at oceanic stations showed higher abundance and the presence of larvae at oceanic stations during two cruises. Larval transport was simulated using outputs of a data assimilation model that represented the flow conditions during each cruise. Higher abundances of larvae of coastal and neritic species at oceanic stations agreed with offshore transport inferred from numerical experiments seeding particles over different spatial scales (stations vs. transects). Satellite images of surface chlorophyll were consistent with the circulation patterns indicated by the model, indicating filaments of shelf waters were transported toward the transects with higher larval abundances. Particle tracking experiments indicated that the northwestern shelf provinces of Perdido, Tamaulipas, and Texas were the main source of propagules to the oceanic region, while shelf provinces of northern Veracruz, Campeche, Yucatan, Louisiana, and Mississippi-Alabama contributed much less. The length and intensity of the shelf front limited ichthyoplankton cross-shelf exchange during some cruises, and mesoscale anticyclonic and cyclonic eddies advected larvae to the deep-water region during others. The agreement between the spatial distribution of fish larvae and the simulated larval transport confirm that circulation models are a valuable tool for examining potential dispersal pathways of neritic species, as long as similar spatial and temporal scales as the ones used in this study are considered.

Connectivity studies are key to comprehending the population dynamics, genetic structure, and biogeography of continental shelf fish populations with pelagic larval stages (Cowen et al. 2006), since larval retention and exchange are two of the main determinants of community structure. They are also important for inferring the resilience potential of communities to acute disturbances such as oil spills (Paris et al. 2020) or natural phenomena such as hurricanes, which are common in the Gulf of Mexico (GoM) (National Oceanic and Atmospheric Administration (NOAA) 2020).

In the nearshore environment, pelagic larval fish transport and dispersion are mainly influenced by the combined effects of tidal, wind and buoyancy driven-currents and bathymetric constraints (Paris et al. 2002). However, in regions with narrow continental shelves and steep slopes, as is the case for western GoM, dispersal distances and transport pathways will also be highly influenced by the interaction between shelf and slope circulation with the mesoscale hydrodynamic processes of deeper waters (Paris et al. 2007).

Vertical larval behavior and larval stage duration (Largier 2003; Leis 2006) will also affect dispersal trajectories and recruitment success. As they develop, larvae increasingly control their buoyancy and position in the water column by swim bladder inflation-deflation (Fuiman 2002). These vertical migratory movements may favor retention in nearshore habitats (Paris and Cowen 2004) that provide suitable habitat as nurseries and for recruitment.

The simulation of Lagrangian trajectories obtained from ocean circulation models allows for the characterization of dispersal pathways of planktonic organisms, as well as for generating estimates of the timing between spawning and

*Correspondence: sherzka@cicese.mx

Additional Supporting Information may be found in the online version of this article.

recruitment (Cowen et al. 2006; Werner et al. 2007; Sanvicente-Añorve et al. 2014). Although open-ocean circulation models have been used to characterize the dispersal pathways of planktonic organisms, their reliability is usually not verified. The comparison of modeled dispersal pathways with species distribution patterns can yield insight into whether these models can be used to examine population connectivity, including multiple spatial and temporal scales, which is typically not feasible with ichthyoplankton cruises.

The aim of the present study was to test if differences in distribution and abundance of neritic fish larvae sampled in the deep waters of the northwestern Gulf of Mexico (NWGoM) can be explained by the oceanic structures present during the cruises. We hypothesized that abundance and spatial distribution of fish larvae of coastal and neritic species in Perdido's deep-water region will be strongly affected by surface currents. We address our goal through the joint analysis of (1) the spatial distribution of fish larvae of coastal and neritic species caught in oceanic waters of the Perdido region, and (2) backward-tracking experiments to simulate the Lagrangian trajectories of passive particles to infer the geographical origin of the larvae. The level of consistency between the results of the biological sampling and the modeling will provide a direct means for evaluating the reliability of larval dispersion pathways that are inferred from circulation models of similar spatial and temporal resolution as the one used in this study.

The focus in the deep northwestern gulf, commonly known as the Perdido region, is due to an increase in hydrocarbon exploration and drilling given the reserves found in the geological formation known as the Perdido Fold Belt (CNH 2019). The impact of an oil spill will depend in part on the level of connectivity and the potential for recolonization, which in bony fish rely on egg drift and larval transport (Paris et al. 2020), and hence regional transport processes underlying population connectivity must be understood. Since numerical models are generally used to infer larval dispersion pathways, it is important to assess whether they provide reliable results by comparing them to actual biological data.

Material and methods

Field sampling

Cruises were conducted along two parallel transects (hereafter referred to as the north and south transects) located in the Perdido region (northern Tamaulipas) of the NWGoM (24°N to 26°N and 94°W to 97°W) (Fig. 1, upper panel). Transects were covered during the Deep-Water Experiment cruises (DWDE), and ran from the edge of the continental shelf (200 m depth), across the slope and toward stations in the gulf's deep-water region. Four cruises were carried out in June (DWDE-1) and October (DWDE-2) 2016, and April (DWDE-3) and November (DWDE-4) 2017. The first cruise included 10 sampling stations (five per transect), while four extra stations were added to the rest of the cruises (14 stations total or 7 per transect). Due to poor weather conditions, one of the stations was not covered in DWDE-3.

Ichthyoplankton samples were collected with a paired bongo net (60 cm diameter and a 335 μm filtering mesh) towed with oblique hauls (45° wire angle) from the surface to 200 m or $\sim$ 5 m above the bottom over the shelf. Tows included a 1 min settling time at the bottom. Nets were towed for an average of 23 (± 6; SD) min at a mean velocity of 2.0 (± 0.4) knots. A flowmeter placed in the mouth of each net was used to estimate the volume filtered during each tow. Each sample was fixed immediately in 7% formalin buffered with sodium borate and transported to the laboratory for identification.

A total of 5810 fish larvae belonging to 295 taxa were recorded and identified the lowest possible taxonomic level based on the descriptions of Richards (2005) and Fahay (2007). Larval abundance was standardized to 1000 m^{-3}. Larval development stages were classified as preflexion, flexion, postflexion, and metamorphosis into early juveniles. To identify the taxa that could serve as tracers of offshore transport, biological and life history information (including the depth distribution of adults, spawning periods and regions, and early life history patterns such as larval behavior and pelagic larval duration [PLD]) were obtained from Richards (2005), Felder and Camp (2009), and Froese and Pauly (2019). Detailed information is provided in Supporting Information Table S1. We selected taxa for which spawning grounds are constrained to bottom depths lesser than 200 m, and here they were classified as coastal-neritic taxa.

Given that our objective is to investigate the connectivity between the continental shelf and open ocean based on the presence of fish larvae of neritic communities (including coral reef-associated taxa) in the deep-water region, stations were assigned into three depth categories: neritic (those located over the continental shelf, depths < 200 m), transitional (located over the upper slope), and oceanic (located in deep waters, at depths > 1000 m) (Fig. 1, lower panel). Since the adults inhabit coastal regions or the continental shelf, the presence of their larvae in oceanic stations is indicative of offshore transport. A nonparametric Kruskal–Wallis test was performed to test for differences between the abundance of coastal and neritic fish larvae caught at oceanic stations for each transect by cruise.

Model experiment

The numerical simulations come from the HYCOM + NCODA Gulf of Mexico 1/25° Analysis: the HYbrid Coordinate Ocean Model Model (HYCOM) is run with the Navy Coupled Ocean Data Assimilation (NCODA) scheme, and forced by the NAVy Global Environmental Model (NAVGEM; see details at the HYCOM Consortium webpage https://www.hycom.org/data/goml0pt04/expt-32pt5). The simulations provide the horizontal components of velocity, u and v (eastward and northward, respectively).

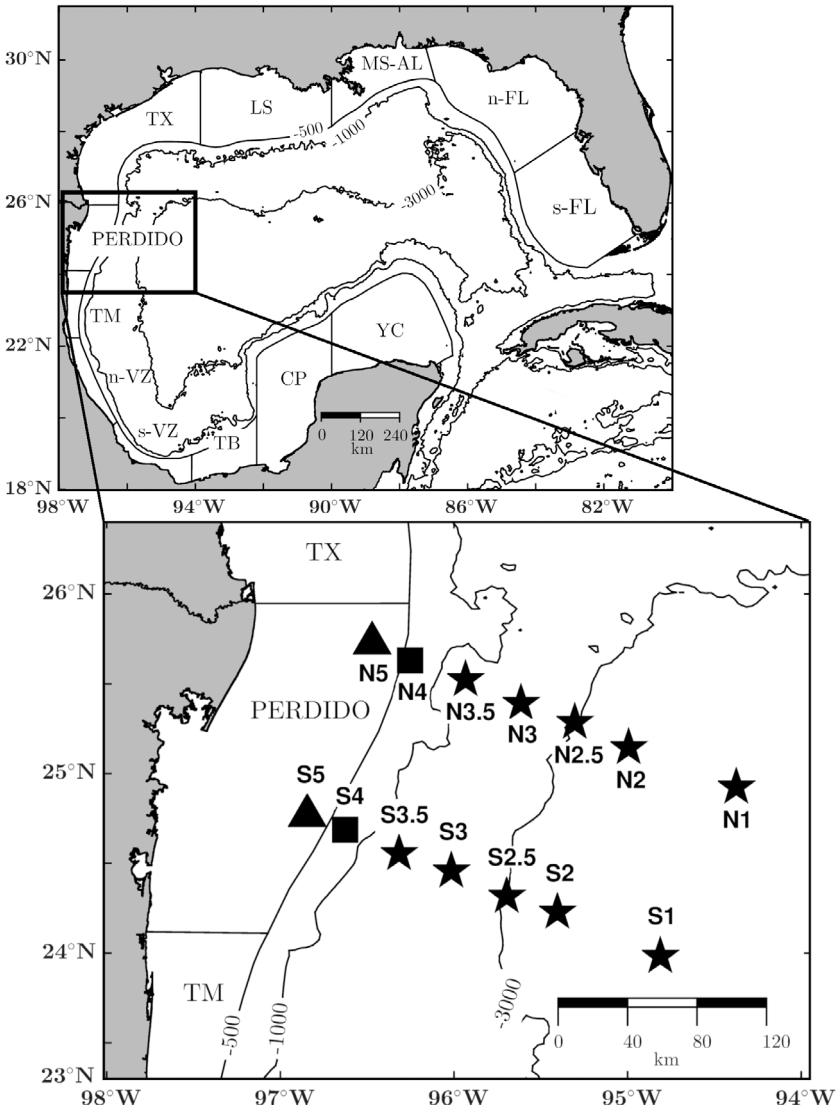

Fig. 1. Map of the Gulf of Mexico with the 12 neritic provinces delimited. Isobaths of 500 (smooth), 1000, and 3000 m are shown. YC, Yucatán; CP, Campeche; TB, Tabasco; s-VZ, southern Veracruz; n-VZ, northern Veracruz; TM, Tamaulipas; TX, Texas; LA, Louisiana; MS-AL, Mississippi-Alabama; n-FL, northern Florida; s-FL, southern Florida. The black box points out the Perdido region where DWDE cruises were carried out. DWDE-1: 21–24 June 2016, DWDE-2: 15–19 October 2016, DWDE-3: 25–28 April 2017, DWDE-4: 07–11 November 2017. Triangles, squares, and stars indicate neritic (< 200 m depth), transitional (depths 200–1000 m), and oceanic (> 1000 m) stations, respectively. Details of sampling stations for each cruise are shown in Fig. 3.

The reproductive strategy of fishes is species-specific and can range from a single event to repeated spawning over a prolonged period of time in batch spawners (Pepin 2002). Larvae collected at each sampling station varied in developmental stage, and could reflect different spawning dates and dispersal histories. Hence, in order to infer the possible origin of the neritic larvae collected during the cruises, particles were seeded at sampling stations on the dates at which the samples were taken on each cruise, and then advected backward in time using the modeled velocity outputs.

A total of 1500 passive particles were released at each of the 17 uppermost layers of the model output (encompassing the surface to 200 m) at the location and time each station was visited. Particles were distributed randomly over a 5 km radius around each station. The particles were advected backward in time from the date on which each station was covered (t = 0 d) until t = −28 d. The values of velocities were obtained from the smallest spatial and temporal resolution available (1/25° horizontal, and 1-h temporal resolution), and advection was calculated using horizontal velocities at each vertical layer with a fourth-order Runge-Kutta algorithm.

Several studies pointed out the necessity to add "motion" to particles to simulate larval swimming behavior to obtain more realistic dispersal pathways, and hence more accurate

evaluations of population connectivity (Cowen et al. 2006; Paris et al. 2007; Werner et al. 2007) since behavior is a potentially important factor that can influence outcomes of the models (Irisson et al. 2009). However, many reports of larval behaviors and swimming speeds are observed in laboratory swimming channels (Fisher et al. 2000; Majoris et al. 2019) and may not be representative of the behavior in the sea (Leis 2006 and references therein). Incorporation of other biological parameters (e.g., egg type, spawning period, mortality, vertical migratory movements, PLD) into particle tracking experiments without consideration of specific early-life-history traits can introduce "noise"'around a relatively simplistic model defined by the oceanographic flow fields and the length of time larvae spend in the plankton (Siegel et al. 2003). Thus, given the uncertainty on traits of most fish larvae species, and due to we conduct our experiment over an ensemble of fish larvae, we decided not to include biological factors, which would likely be biasing our results if incorporated on a species-specific basis. Nevertheless, to address the potential effects of vertical migration, dispersal pathways were tracked using the 17 upper-layers, which encompass from 0 to 200 m water depth. This layer encompasses the depths through which fish larvae usually move to feed on zooplankton (Auditore et al. 1994) and to avoid predation (Jellyman and Tsukamoto 2005).

Since population connectivity increases with a longer PLD (Sponaugle et al. 2002), its choice will have a strong impact on modeling results. For coastal and neritic species, PLD typically varies from a few days or weeks to ~ 3 months (Sale 1991 and references therein; Macpherson and Raventos 2006; Beldade et al. 2007; Puebla et al. 2012). The maximum number of days (28) used in this study was selected based on a typical PLD for fish larvae of some of the coastal and neritic species documented in the GoM (Zapata and Herrón 2002; Rooker et al. 2004). Given that species with very different PLDs have broadly overlapping dispersal ranges (Jones 2015), the use of a common PLD for several taxa may not necessarily imply inaccurate estimates of dispersal pathways.

Since ocean currents are inherently chaotic, this leads to uncertainty in the larval pathways inferred from the velocity fields of circulation models (Christensen et al. 2007). The reliability of backward particle trajectories was evaluated by tracking them from their final position in the backward in time simulation forward in time, and evaluating the percentage of particles returning to the source region. We also compared the results of this analysis using the velocity fields with hourly and daily resolutions. A higher mean percentage (± SD) of particles advected backward in time and then forward again over 28 d returned within 5 km of their original release site with the hourly horizontal velocities (hourly: 90.6 ± 16.6; daily: 25.1 ± 26.4). The results of backward-forward hourly simulations seem to reduce errors, supporting the use of hourly velocity fields on our modeling experiments.

Due to the chaotic nature of ocean currents (Johnson et al. 2013), a large number of particles is required for robust statistics in connectivity scenarios (Hamilton et al. 2016). Two sampling units of different spatial scales were used to analyze the particles' trajectories: (1) whole transects and (2) pooling data from adjacent stations located over the lower slope (Sta. 3 and 3.5), the abyssal plain (Sta. 2 and 2.5) and the most oceanic and deepest station (Sta. 1; Fig. 1, lower panel).

Thus, for each cruise and sampling unit, the total number of particles at any given time (t), sampled hourly between $T = -28$ d and $t = 0$ d is N, where $N = 1500$ particles × 17 vertical layers × S number of stations comprising the sampling unit. From the coastline to the upper continental slope, we defined 12 provinces around the GoM as possible sources of coastal and neritic larvae; provinces were delimited using the smoothed 10 and 500 m isobaths as internal and external limits (Fig. 1, upper panel). This division was chosen because oceanic fronts in the western GoM that can isolate shelves from the deep-water region are typically steered by the well-defined shelf break and the steep upper continental slope (Belkin et al. 2009). In addition, provinces were designed to contain known circulation patterns, such as seasonal convergences in the NW and southern shelves (e.g., Martínez-López and Zavala-Hidalgo 2009), the influence of the BoC cyclonic gyre circulation on the western slope and shelf (e.g., Pérez-Brunius et al. 2013; Lara-Hernández et al. 2019), the western boundary current (Sturges 1993), the isolated west Florida shelf (Olascoaga et al. 2006), and the Mississippi river delta. Last, the large area covered by the provinces yield a sufficient number of particles (hundreds) so as to establish a robust statistical analysis.

For each cruise and sampling unit, the number of particles present in the water column (0–200 m) in a given province j at a given time t were counted (m_j (t), with j = {1, 2, … 12}), where t is a step function counted backward hourly until time $t = T$ (i.e., t = {−28: 1/24: 0} d). The proportion of particles in each coastal and neritic province of the entire gulf was calculated with respect to the total number particles released as:

$$\mathbf{P}(\boldsymbol{t}) = \mathrm{M}(t)/N, \text{where } \mathrm{M}(t) = \sum_{j=1}^{12} m_j(\mathrm{t}) \quad (1)$$

where M(t) is the total number of particles that had a neritic origin, and N is the total number of particles released in the 17 uppermost layers as described above. Hence, $\mathbf{P}(\boldsymbol{t})$ is an estimate of the likelihood that neritic-larvae of age t could be found on a given transect of a particular cruise. $\mathbf{P}(\boldsymbol{t})$ reflects the proportion of particles that were located in the sampling unit at time $t = 0$ that can be traced to any of the neritic provinces of the GoM t days before the cruise. If all particles released in the sampling unit were traced back to the neritic region t days earlier, $\mathbf{P}(\boldsymbol{t}) = 1$, if all particles released in the sampling unit were traced back to deep waters, $\mathbf{P}(\boldsymbol{t}) = 0$. This proportion changes with the time used to backtrack the position to when the simulated larvae "were spawned." Although we recorded the larvae's development stages, under natural conditions stage duration is very variable because growth rates are strongly influenced by environmental factors (Houde 1989). Since the exact age of each larva was unknown, we assume it

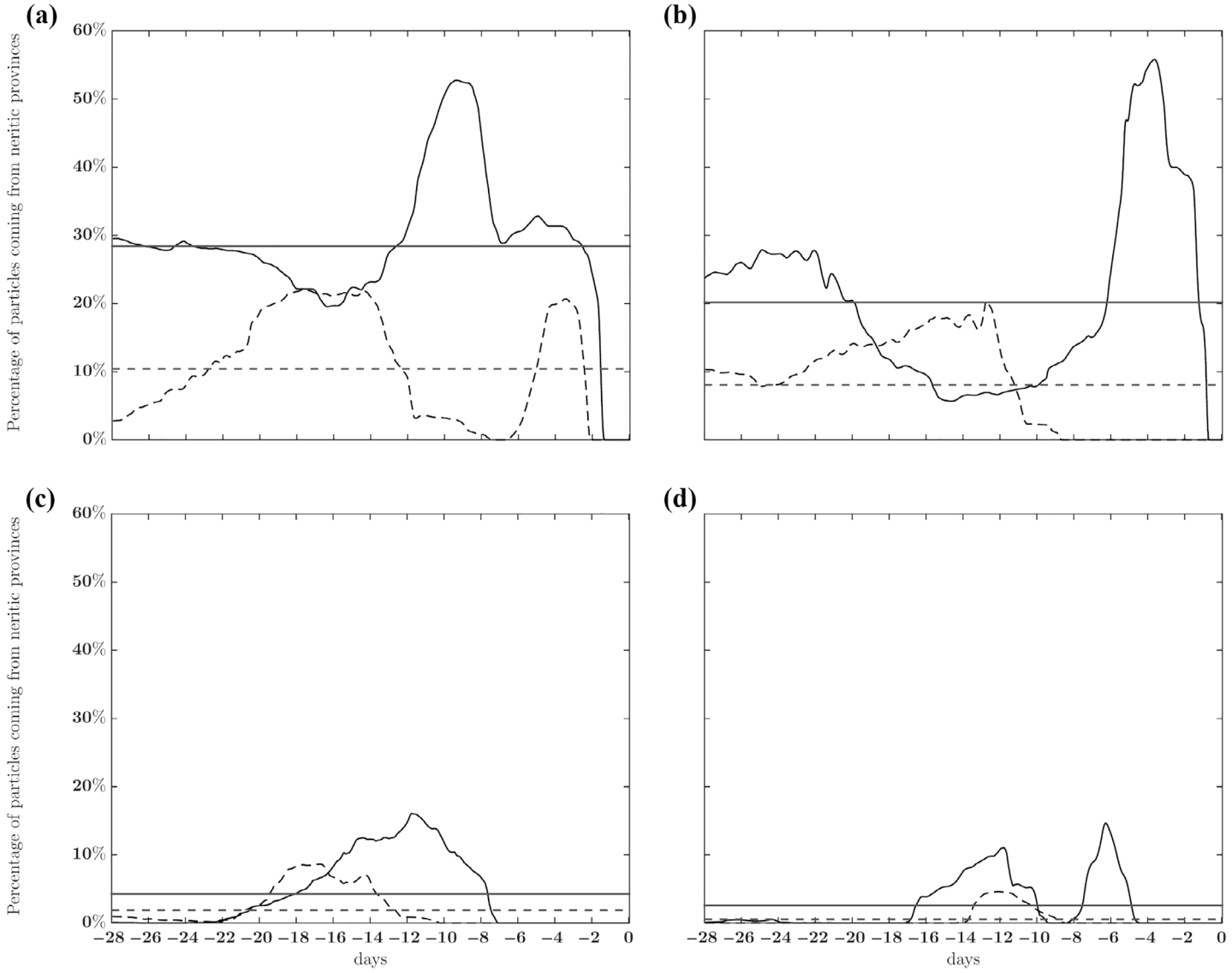

Fig. 2. Percentage of particles coming from the coastal and neritic regions with respect to all particles released **(P)** as a function of backward time (larval "age"). The results for the north transect (solid line) and south transect (dashed line) for each cruise are depicted: (**a**) DWDE-1 (June 2016), (**b**) DWDE-4 (November 2017), (**c**) DWDE-2 (October 2016), and (**d**) DWDE-3 (April 2017). Horizontal solid and dashed lines depict the time-averaged (**P**) proportion of particles for the north and south transect, respectively, that were calculated for each cruise.

ranged between 0 and 28 d (Fig. 2), and used the time average of this proportion over the entire period (T = 28 d) as a metric:

$$<\mathbf{P}(\mathbf{t})> = \frac{1}{T}\int_0^T P(t)dt \approx \frac{1}{T}\sum_{t=1}^{T} \mathrm{P}(t)\,\Delta t, \text{with } \Delta t = 1\,\mathrm{h} \qquad (2)$$

Rewriting time in terms of $t = k\ \Delta t$, with k = {1, 2, 3, … K}, and $K = \frac{T}{\Delta t} = 672$

$$\mathbf{P} = <\mathrm{P}(t)> \approx \frac{1}{K}\sum_{k=1}^{K} P(k) \qquad (3)$$

In other words, we calculated the average of the hourly proportions calculated over a 28 d period, with the maximum "age" of the larvae (T) corresponding to a 28 d PLD.

The temporal evolution and the time-averaged proportion of particles coming from the neritic region with respect to all particles released at each whole transect and cruise (**P**) is presented in Fig. 2. Consistent results were obtained for both sampling units, as discussed later, so the analysis will focus at the transect level. The reader can consult the results for the smaller-scale spatial units (lower slope, abyssal plain, and oceanic station) in Supporting Information Fig. S1.

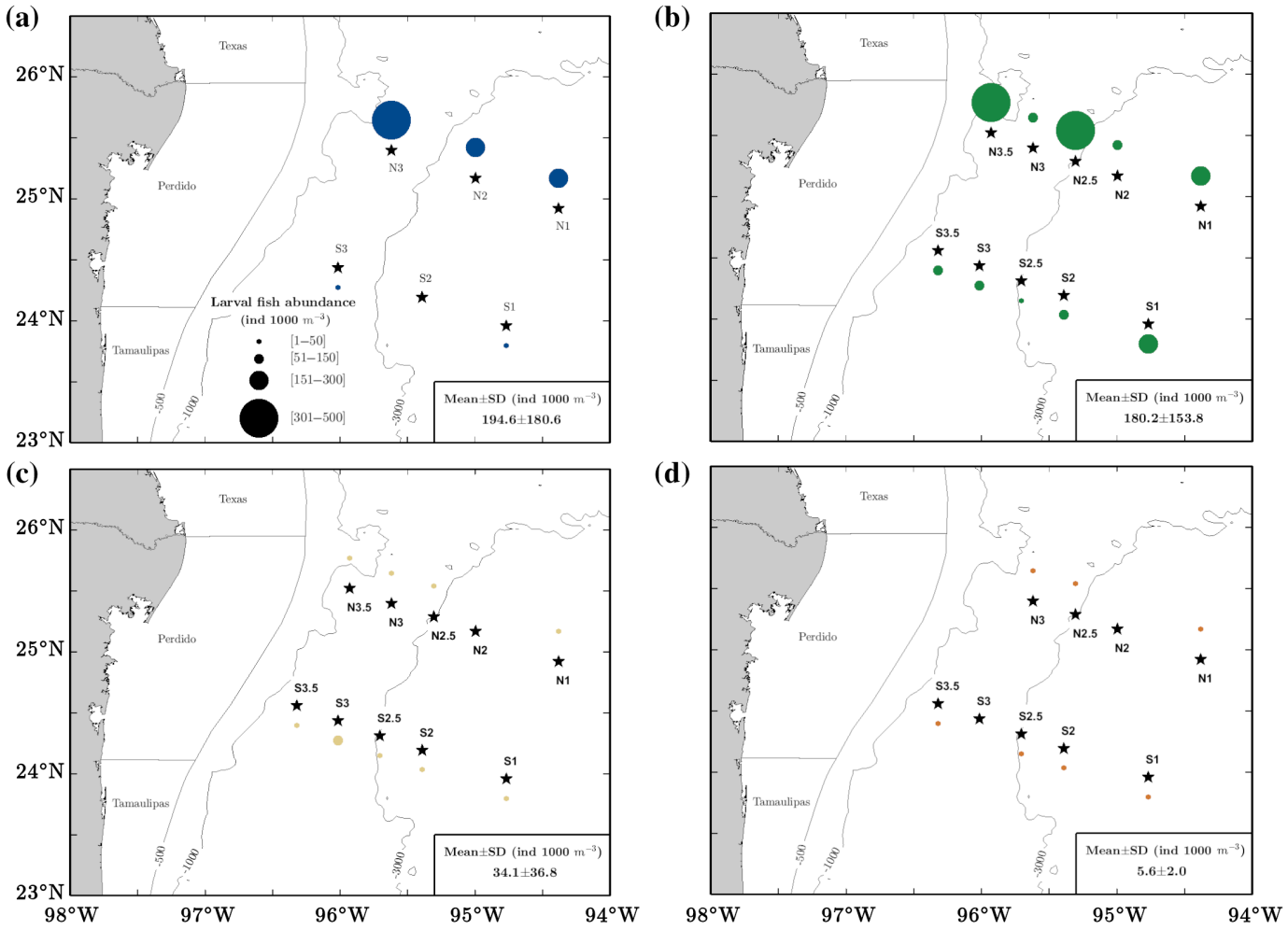

Fig. 3. Distribution of the standardized abundance (individuals per 1000 m^{-3}) of coastal and neritic fish larvae (circles) caught in oceanic stations (stars, depths > 1000 m) for different cruises: (**a**) DWDE-1 (June 2016), (**b**) DWDE-4 (November 2017), (**c**) DWDE-2 (October 2016), and (**d**) DWDE-3 (April 2017). Isobaths of 500 (smooth), 1000, and 3000 m are shown.

The metric **P** indicates the cruise and transect in which a greater proportion of coastal and neritic larvae are expected to be found, but does not provide the provinces of origin. An analogous analysis can be made to obtain the spatial distribution of the $M(t)$ particles of neritic origin among the 12 provinces, by examining the proportion of particles at time t (larval "age") found in a given province j, $j = \{1, 2, \ldots 12\}$:

$$\mathbf{P_j}(t) = m_j(t)/\mathrm{M}(t), \tag{4}$$

and the temporal average of that proportion is then:

$$\mathbf{P_j} = <\mathrm{P_j}(t)> \frac{1}{K}\sum_{k=1}^{K} P_j(k) \tag{5}$$

This metric is an estimate of the likelihood that province j is the source of the neritic particles with "age" t that are found on a given transect and cruise.

The proportion of particles originating from neritic provinces for each cruise and sampling unit was correlated with the relative abundance of coastal and neritic larvae to test for consistency between biological data and the numerical circulation modeling. Pearson's correlation coefficient was used to examine the strength of the relationship between the richness of coral reef fish larvae captured in each transect and cruise, and the number of provinces that harbor coral reef habitat and/or oil and gas platforms (provinces of Veracruz, Campeche, Yucatan, Texas, Louisiana), which could act as their possible source of propagules.

In addition, surface velocity fields from the model outputs were used to characterize the flow patterns that give raise to

Table 1. Standardized abundance (ind 1000 m^{-3}) of coastal and neritic fish larval families caught at oceanic (depths > 1000 m) stations in the north and south transects for each cruise.

	North				South			
Family	**DWDE-1**	**DWDE-2**	**DWDE-3**	**DWDE-4**	**DWDE-1**	**DWDE-2**	**DWDE-3**	**DWDE-4**
Balistidae	2.0			3.8				
Bothidae	21.2	10.8	6.6	7.6		48.6	3.2	37.2
Bregmacerotidae	430.7	3.2		231.9	12.6			47.8
Bythitidae						3.0		
Callionymidae				7.6		9.2		
Carangidae	5.2							
Cynoglossidae	4.1			18.9				
Eleotridae							3.2	
Engraulidae	61.3	47.9		7.5			4.2	10.9
Gerreidae	25.3							
Gobiesocidae								7.4
Gobiidae	186.0	27.7	7.0	925.3	9.0	51.1	3.8	262.0
Kyphosidae							5.3	
Labridae		6.8				26.4		11.8
Megalopidae						6.6		
Microdesmidae	67.7	7.1		14.4	3.0			7.9
Moringuidae				7.5				14.9
Ophidiidae				7.5				
Paralichthyidae	118.3			140.2	9.0	7.1		8.0
Pomacentridae	2.6							
Scaridae		11.6	3.3	3.8		66.9		18.7
Sciaenidae				33.9				
Serranidae								7.5
Sphyraenidae	7.7							
Synaphobranchidae	2.0							
Synodontidae						3.2		
Tetraodontidae	5.2			11.3		3.9	2.7	
Percent of neritic taxa relative to total larval abundance	23.8	6.8	0.8	48.7	1.7	4.6	1.8	30.1

the spatial distribution of the origin of modeled larvae for each cruise and transect. The relative vorticity was used to identify oceanic fronts and eddies, and was calculated as:

$$\omega = \frac{\partial v}{\partial x} - \frac{\partial u}{\partial y} \quad (6)$$

where u and v are the surface velocity components along the east–west and north–south directions.

Chlorophyll surface

Offshore transport in the NWGoM can be traced by remote sensing of shelf water plumes with high chlorophyll concentration that are entrained seaward (Biggs and Müller-Karger 1994). The level-4 (gap-free gridded data after validation process) surface daily chlorophyll *a* (Chl *a*) concentration (product identifier: oceancolour_glo_chl_l4_rep_observations_009_082) provided by Copernicus Marine Environment Monitoring Service (CMEMS) was used in this study.

Results

Larval fish identification

Larvae of 42 taxa belonging to 27 families with a coastal and neritic adult stage were caught at the oceanic stations (Table 1, Supporting Information Table S1). Generally, the most abundant and better-represented families were Bothidae, Bregmacerotidae, Engraulidae, Gobiidae, and Paralichthyidae. Preflexion and flexion larvae were dominant in all cruises. On average, 35.1% of fish larvae were in the preflexion, 54.5% in flexion, 10.0% in postflexion, and 0.4% in metamorphosis.

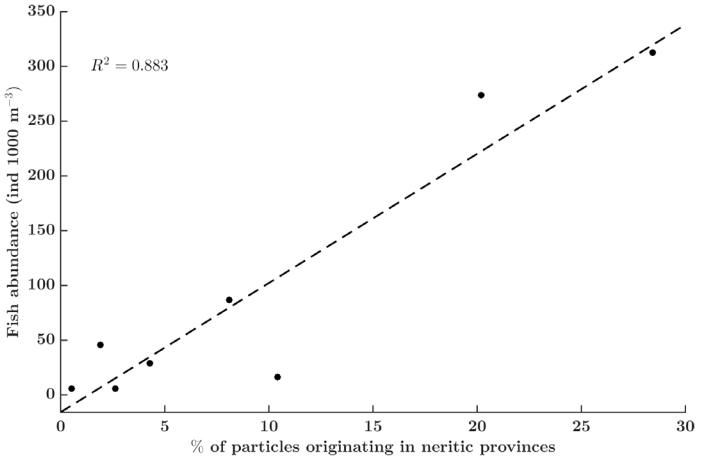

Fig. 4. Relationship between the average percentage of particles originating in neritic provinces relative to all particles released and the average abundance of fish larvae caught at oceanic stations at each of two transects covered during four cruises in the NWGoM.

At a lower identification level, *Bothus* spp., *Engraulis eurystole*, *Ctenogobius* spp., and *Gobionellus* spp. were identified during the four cruises (Supporting Information Table S1), and could be used as tracers of offshore transport year round. On the other hand, although the distribution and abundance of taxa belonging to reef-associated species (e.g., *Ctenogobius* spp., *Sparisoma* spp., *Bodianus rufus*, *Sphoeroides* spp., *Calllionymus bairdi*) varied between transects, they were more abundant during the second and fourth cruises (Supporting Information Table S1). There was a positive linear correlation between the richness (total number of coral reef families, genera, or species; Supporting Information Table S1) in each transect and cruise and the number of provinces that have coral reef habitat and/or oil and gas rigs, which could act as sources of propagules ($r = 0.812$, $p = 0.014$).

Fish larvae abundances and simulated larval transport

The average standardized abundances of fish larvae classified as coastal and neritic caught at oceanic stations varied significantly between transects during DWDE-1 (Kruskal–Wallis test, $n = 6$, df = 1, $H = 3.857$, $p = 0.049$) and DWDE-4 (Kruskal–Wallis test, $n = 10$, df = 1, $H = 4.811$, $p = 0.028$) and were higher in the northern transect during both cruises (Fig. 3a,b). In contrast, the abundances were much lower during the other two cruises (Fig. 3c,d), and there were no differences between transects (DWDE-2, Kruskal–Wallis test, $n = 10$, df = 1, $H = 0.273$, $p = 0.601$; DWDE-3, Kruskal–Wallis test, $n = 9$, df = 1, $H = 0.015$, $p = 0.902$).

Analogous results were found for the time-average proportion of particles originating from neritic provinces for each cruise and transect. That means that average **P** values were higher for the first and fourth cruises (Fig. 2). There was also agreement in that a higher **P** value was found for the north transect for the cruises that exhibited significant differences in fish larvae abundance between transects. The smaller spatial sampling units also show a higher proportion of particles for the first two cruises and for the northern transect (Supporting Information Fig. S1). The smaller-scale unit indicated that the higher larval abundance found in the most oceanic station (S1) of the southern transect during DWDE-4 is also associated with a higher proportion of particles with neritic origin (Fig. 3b and Supporting Information Fig. S1b). For both sampling units, there was a significant positive linear relationship between larval fish abundance and numerical experiment results ($p < 0.001$; Fig. 4 and Supporting Information Fig. S2).

Figure 2 presents the percentage of particles coming from the coastal and neritic regions with respect to all particles released as a function of larval "age" (**P(t)**) for the north and south transect for each cruise, and can be used to examine how varying larval stages and/or PLD would modify the estimate of the average likelihood of particles coming from neritic regions. Similar significant correlations ($p < 0.005$) between the biological outcomes and numerical experiment results were found using shorter averaging periods ($T = 7$, 14, and 21 d in Eq. 2; results not shown), which represent different larval stages or PLDs shorter than 28 d.

Backward particle tracking results

The temporal evolution of **P**, as in the case of their average values mentioned above, varied both between sampling units and among cruises. The DWDE-1 and DWDE-4 cruises showed a broad range of modeled larval "ages" wherein particles could come from neritic provinces, while in DWDE-2 and DWDE-3 the range of larval "ages" coming from neritic provinces were shorter (Fig. 2 and Supporting Information Fig. S1). Note that the proportions of larvae originating in coastal and neritic provinces were generally much higher during the DWDE-1 and DWDE-4 cruises compared to the other two cruises, regardless of larval "age." The higher average proportion (> 20%) were found in the northern transect for both cruises (Fig. 2). This was particularly noticeable in N3 during DWDE-1 and N3 + 3.5 during DWDE-4, where highest proportions were observed starting in day 2 (Supporting Information Fig. S1). The distribution of the particles of neritic origin among the 12 provinces, that is, the time-averaged proportion of neritic particles for each province ($\mathbf{P_j}$), is shown in Fig. 5.

During the first cruise, the likelihood of arriving from the neritic zone was higher in the northern transect (Figs. 2a, 5a left), in agreement with the larval fish spatial distribution (Fig. 3a). For the north transect, the time-averaged proportion of released particles originating from neritic provinces was 28.4% (Figs. 2a, 5a left), while for southern stations it was just 10.4%. (Figs. 2a, 5a right). The main source of particles was the Perdido neritic province (north: 53.7% of all released particles, south: 48.1%) followed by southern Tamaulipas (north: 21.3%, south: 47.8%), northern Veracruz (north: 17.9%, south: 3.5%), and the Texas shelf (north: 7.1%, south: 0.6%). Likewise, the results of the particle tracking experiment for

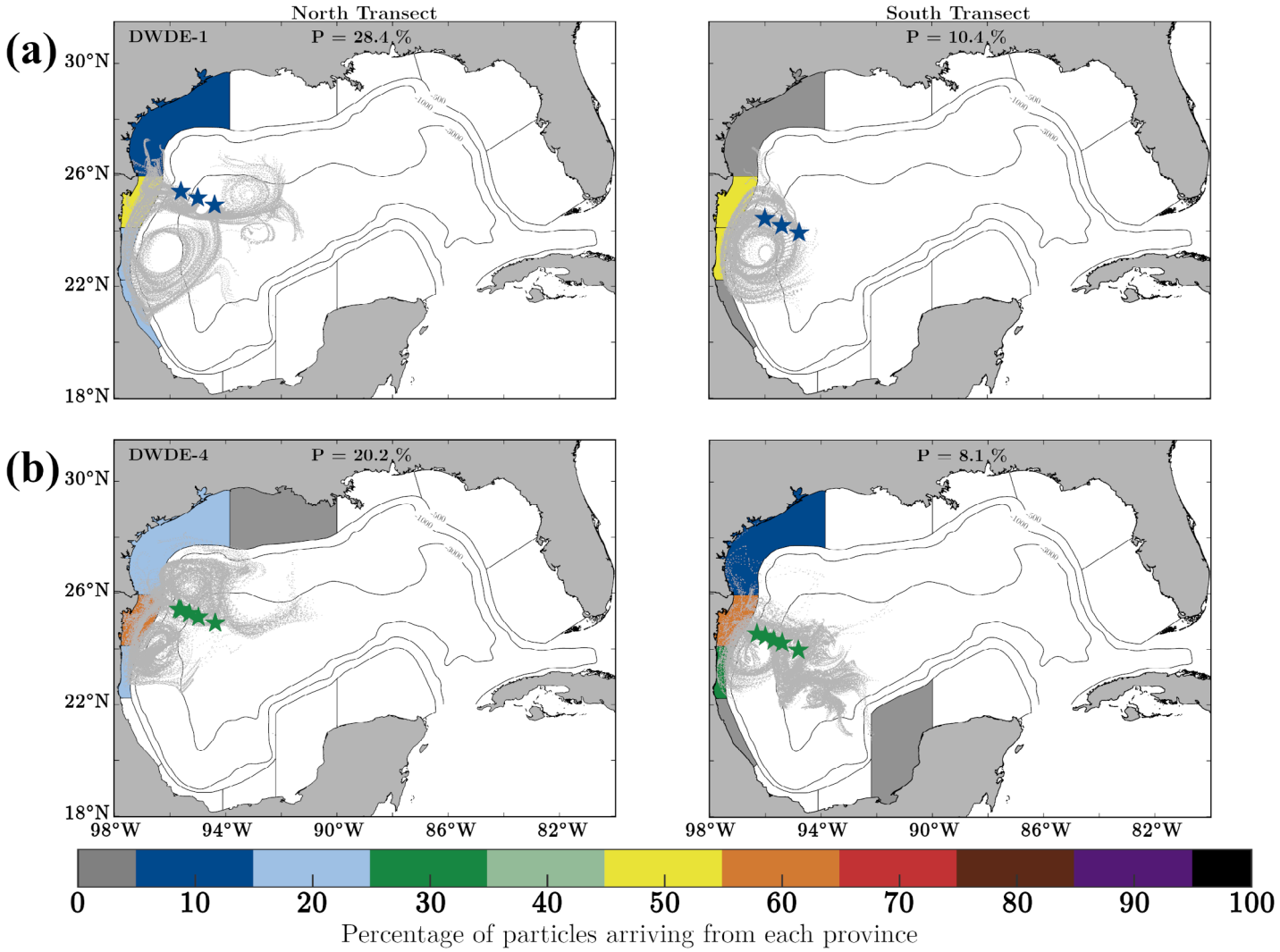

Fig. 5. Results of the particle tracking experiments. Stars indicate the positions of stations in each transect at which particles were released from the surface to 200 m (north: left panels, south: right panels) for cruises: (**a**) DWDE-1 (June 2016), (**b**) DWDE-4 (November 2017), (**c**) DWDE-2 (October 2016), and (**d**) DWDE-3 (April 2017). Gray dots show the trajectories of particles during the 28 d of simulation. The time-averaged proportion of neritic particles for each province ($\mathbf{P_j}$) is shown according to color scale. The time-averaged proportion of particles coming from all neritic regions (**P**) is shown in the header. Smoothed isobaths correspond to 500, 1000, and 3000 m.

DWDE-4 (Fig. 5b) coincided with the distribution of fish larvae (Fig. 3b); the likelihood of finding larvae of neritic origin was greater for the north (20.2%) than the south transect (8.1%). The major sources of virtual larvae were Perdido, Texas, and Tamaulipas, whereas a scant quantity of particles came from the provinces of Louisiana (Fig. 5b left), as well as northern Veracruz and Campeche (Fig. 5b right).

For the second cruise (DWDE-2), the likelihood of originating from neritic provinces was substantially lower than for DWDE-1 and DWDE-4; the time-averaged proportion of particles originating from neritic provinces was low for the north (4.3%) and south (1.9%) transects (Fig. 5c left and right, respectively). This agrees with the lower larval fish abundance of neritic taxa caught at oceanic stations during this cruise (Fig. 3c). Although both transects displayed a similar pattern regarding the origin of the particles for all stations, with the Perdido and Tamaulipas provinces as the main sources, there were differences in the potential origin of dispersed particles to the deeper oceanic stations. The farthest station from the shelf in the south transect had Campeche, Yucatan and Louisiana provinces as the main sources of particles, whereas Tamaulipas and Mississippi-Alabama were the primary source for stations in the north transect. In the case of the third cruise (Fig. 5d), few particles originated in neritic provinces for both transects (north: 2.6%, south: 0.5%), which agrees with the limited presence of neritic larvae sampled (Fig. 3d). The

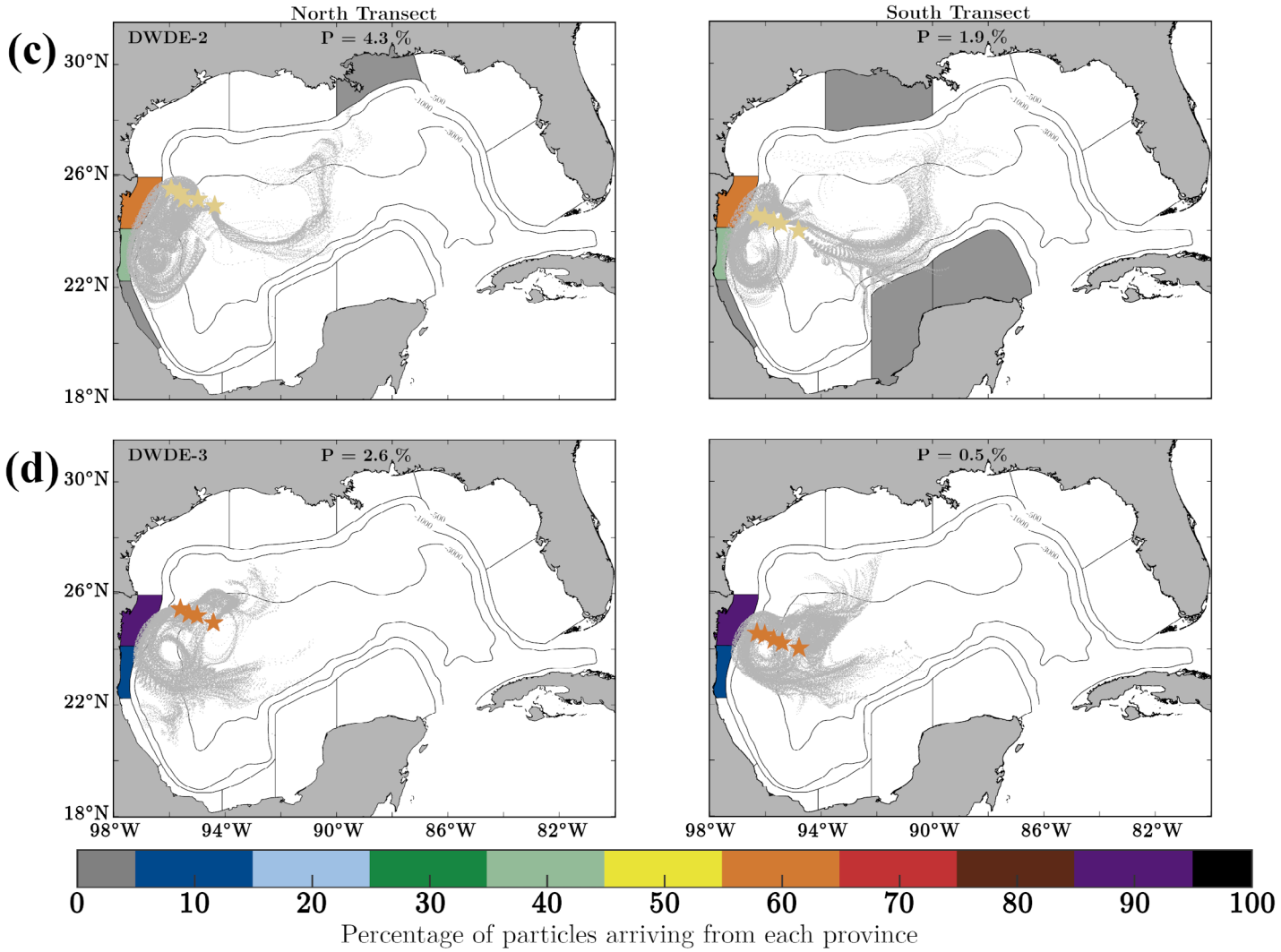

Fig. 5 (Continued)

few particles that arrived at the oceanic stations came from the Perdido and Tamaulipas shelf provinces.

Fish larvae distribution and observed circulation patterns

Dispersal pathways from the different shelf provinces of the GoM to the oceanic Perdido stations were different for each cruise, since the sources of virtual larvae will depend on the circulation patterns present 28 d before and until the time at which each cruise took place. Snapshots of the relative vorticity and surface velocity fields are shown in Fig. 6 for each cruise.

In the first cruise, virtual particle trajectories suggest a greater quantity of propagules coming from neritic provinces in the north transect (Fig. 2a and Supporting Information Fig. S1a), in agreement with fish larval abundance (Fig. 3a). The influence of an anticyclonic eddy, located approximately at 23°N (Fig. 6a) and which persisted during the cruise, is likely the most relevant mesoscale oceanographic structure driving the dispersal pathways from the continental slope and neritic provinces of Perdido and southern Tamaulipas provinces. The front that ran roughly parallel and between the north and south transects 1 month before and during the cruise (Fig. 6a) could be responsible for the great difference in fish abundance between the northern and southern stations (Fig. 3a). Similarly, during the last cruise (DWDE-4), there was a higher abundance of coastal and neritic taxa in the northern stations (Fig. 3b), which agrees with the high percentage of particles from neritic provinces obtained from particle

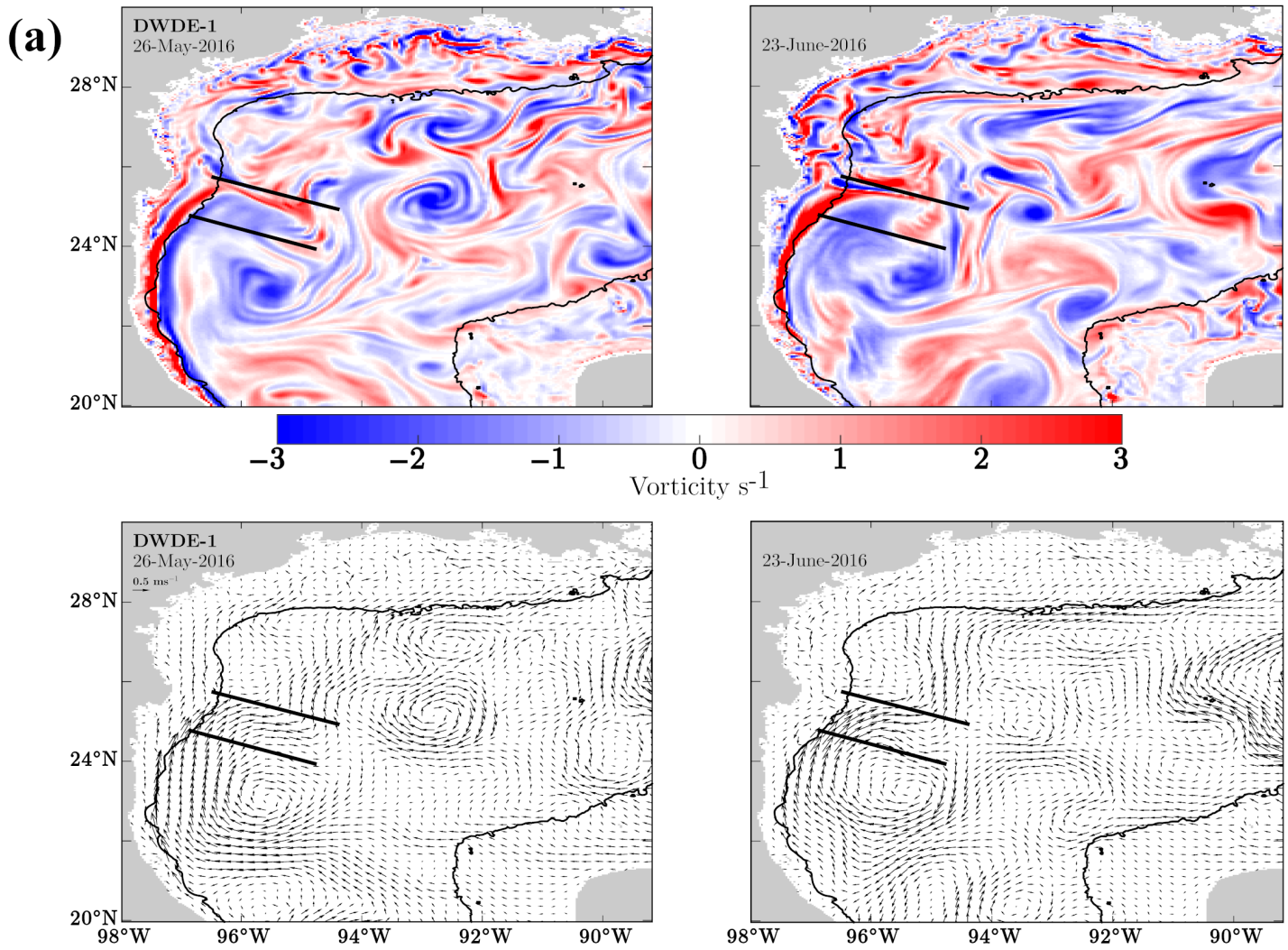

Fig. 6. Snapshots of the relative vorticity (s^{-1}, upper panels) and surface velocity fields from the model outputs (m s^{-1}, lower panels) 28 d before each cruise (left panels) and at the time of the cruise (right panels): (**a**) DWDE-1 (June 2016), (**b**) DWDE-4 (November 2017), (**c**) DWDE-2 (October 2016), and (**d**) DWDE-3 (April 2017). Black parallel lines indicate the north and south transect positions (the specific location of each station is shown in Fig. 3). The isobath of 200 m is depicted with a black line.

backtracking (Figs. 2b, 5b, and Supporting Information Fig. S1b). The greatest mean abundances observed in the northern transect stations during this cruise is probably linked to the presence of an eastward jet across the shelf 2 weeks before the start of the cruise. This was generated by the presence of an anticyclonic structure toward the south and a cyclonic structure toward the north that converged within the sampling region (Fig. 6b). The jet acts as a mechanism for larval export from the western shelf to the open ocean. Offshore transport across the shelf break due to these cyclone/anticyclone eddy pairs is confirmed by the chlorophyll filaments observed in the region (Fig. 7). Specifically, a greater presence of shelf waters flowing into the Perdido oceanic region can be seen in the first (Fig. 7a) and last (Fig. 7b) cruises, notably for the northern transect.

The biological and physical results are also in agreement for the second and third cruises. In both cases, there was a much lower larvae abundance and time-averaged proportion of passive particles coming from the neritic provinces (DWDE-2: Figs. 2c, 3c, 5c, Supporting Information Fig. S1c; DWDE-3: Figs. 2d, 3d, 5d, Supporting Information Fig. S1d). In fact, the proportion of particles for any given time between 0 and 28 d is low compared to the other two cruises (Fig. 2 and Supporting Information Fig. S1). For DWDE-2, this may be related to the high intensity of the east–west front north of the Perdido region, which would confine the transport of

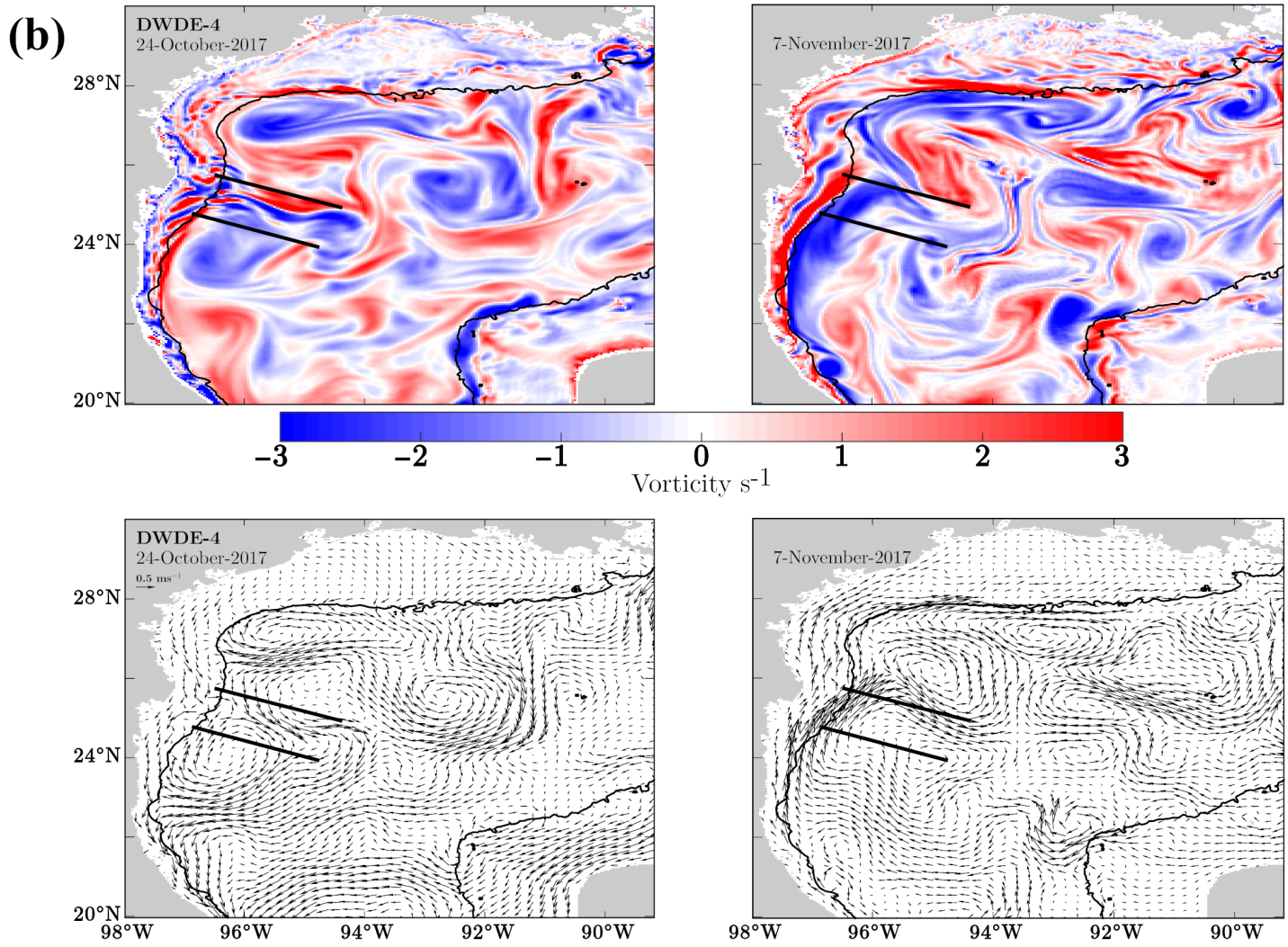

Fig. 6 (Continued)

coastal and neritic larvae to a location north of the sampling stations (DWDE-2: Fig. 6c). The higher abundance of fish larvae found in the southern transect (Fig. 3c) could be attributed to the presence of a weak shelf front during the month prior to the cruise, allowing for more cross-shelf transport to occur. In addition, during the cruise toward the south of the sampling region there was an anticyclone close to the slope, which could transport fish larvae from the shelf edge of the western neritic provinces of Perdido and southern Tamaulipas toward the deep-water region. The lowest fish abundances found during DWDE-3 (Fig. 3d), seems to be related to the long-lived shelf front at around 26°N (Fig. 6d), which would act as a barrier to dispersal between the western neritic provinces (Perdido, Tamaulipas, Veracruz, and Texas shelves) and Perdido oceanic waters. The highest offshore transport detected from chlorophyll filaments in the second (Fig. 7c) and third (Fig. 7d) cruises were further to the north of the survey region, suggesting no shelf waters were transported to the oceanic stations in neither of these two cruises. The slightly higher abundance found in the Sta. S3 during DWDE-2 (Fig. 3c) could be attributed to a weak chlorophyll filament that reached the site (Fig. 7c).

Discussion

Circulation patterns and fish larval distribution

While reproductive cycle seasonality is the first prerequisite determining the presence of larvae of coastal and neritic taxa, our results indicate that the dominant mechanisms controlling ichthyoplankton transport were the length and intensity of the shelf front that limited cross-shelf exchange, and the

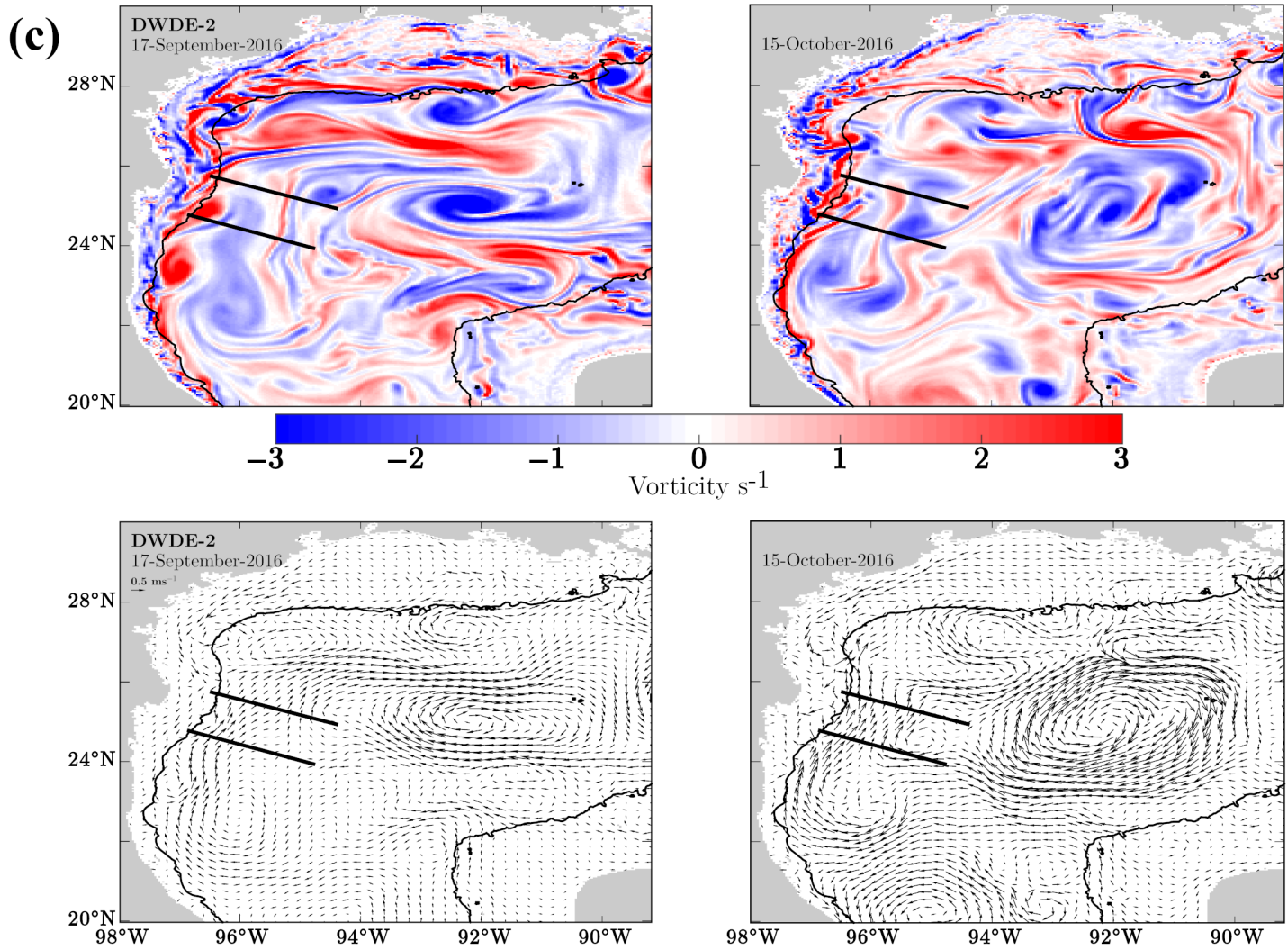

Fig. 6 (Continued)

presence of mesoscale anticyclonic and cyclonic eddies that advected larvae from the shelf to the deep-water region.

The interaction of anticyclonic and cyclonic eddies leading to an eastward transport (as observed during the cruise DWDE-4 both in fish larvae abundance as well as by the chlorophyll filaments) in the NWGoM has been described previously (e.g., Biggs and Müller-Karger 1994; Martínez-López and Zavala-Hidalgo 2009). On the other hand, the presence of along-shelf fronts in the western GoM (as observed during DWDE-3) has been previously described (Zavala-Hidalgo et al. 2003; Gough et al. 2019), which likely constrains the exchange of larvae between the shelf and the deep-water region.

Understanding the connectivity level of fish communities among different subregions within the same domain is key to study the resilience potential of continental shelf fish species (Paris et al. 2020). The interaction of eddies with the slope could enhance the larval dispersion to deep waters, while a strong shelf-break front could encourage retention of larvae within the neritic region, thereby contribution to local population replenishment and/or favoring the connectivity between the shelf provinces of Veracruz, Tamaulipas, Perdido, and Texas.

Origin of coral reef-associated fish larvae

Different shelf provinces of the GoM harbor both coral reef habitat (Veracruz, Campeche, Yucatan: Liddell 2007, and Texas–Louisiana: Nash et al. 2013) and oil and gas platforms (Bay of Campeche: CNH 2019, and Texas–Louisiana: Sammarco 2014), which could provide suitable habitat for the settlement by reef fish (Barker and Cowan 2018). The high correlation between coral reef taxa species richness and the particle backtracking results is remarkable and provides further

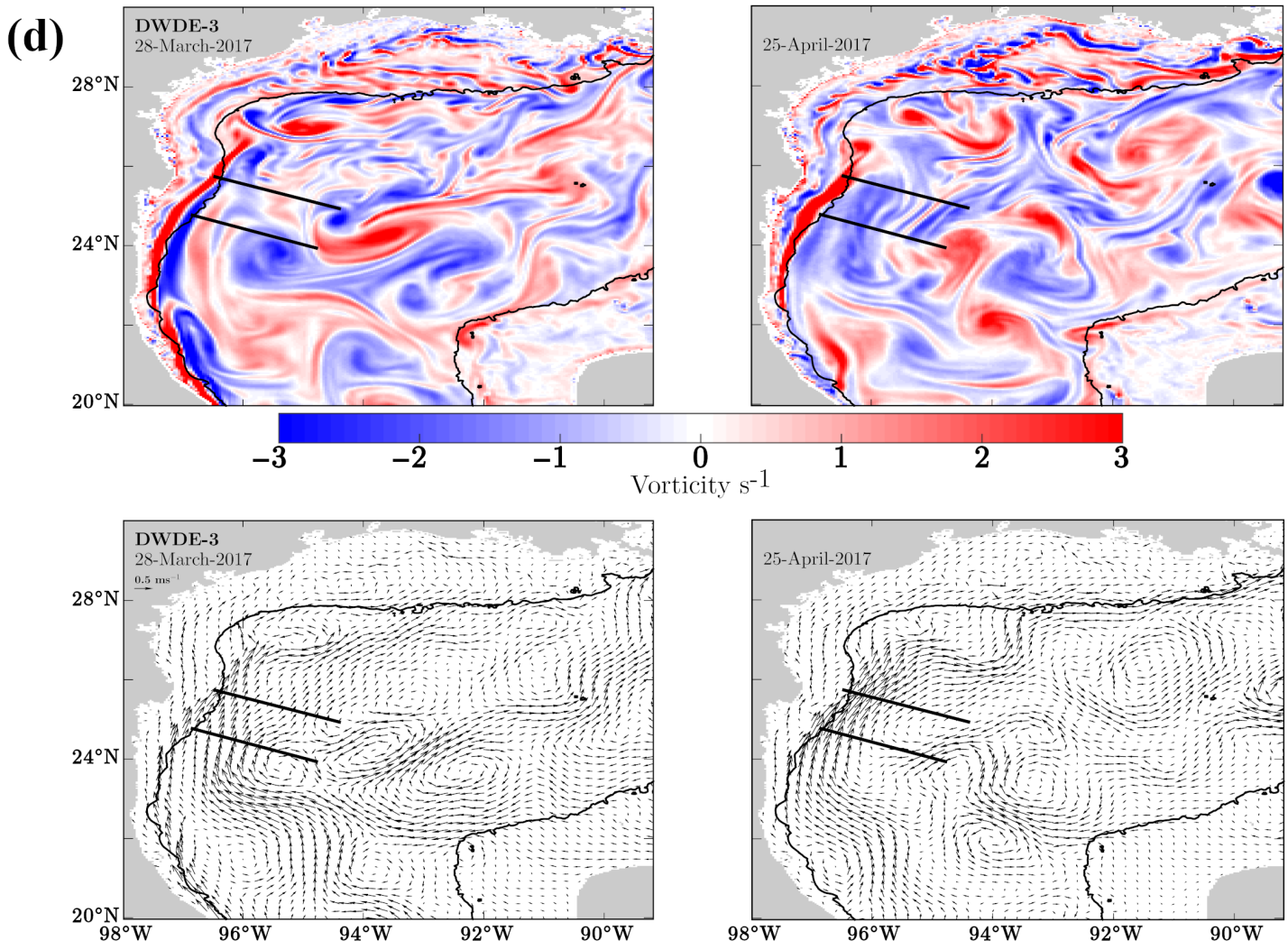

Fig. 6 (Continued)

support for the use of the model to infer their dispersal pathways.

During the first cruise, reef-associated fish larvae (*Balistes capriscus*, *Coryphopterus* spp., *Ctenogobius* spp., *Chromis multilineata*, *Canthigaster* spp., and *Sphoeroides* spp.) were mainly found at the northern transect, whereas only *Coryphopterus* spp. was caught in the southern transect (*see* Supporting Information Table S1). This finding agrees well with the particle backtracking simulation, since the likelihood of larvae originating from the Texas and northern Veracruz continental shelves was higher in the northern transect. The pathways followed by propagules coming from the Texas inner shelf southward, crossing the Perdido shelf and then transported offshore agrees with a recent 28 d numerical simulation study performed with passive tracers also in the NWGoM (Gough et al. 2019). The slightly higher abundance of coral reef-associated fish larvae in the northern transect during the last cruise (DWDE-4, Supporting Information Table S1) was also in agreement with its corresponding particle backtracking simulation, since the likelihood of coming from the Texas and Louisiana in the case of the north transect (Fig. 5b, left) was higher than the likelihood of coming from Texas and northern Veracruz for the south transect (Fig. 5b, right).

The likelihood of reef larvae originating in provinces with reefs in the second particle backtracking simulation was higher for the southern stations (Fig. 5c), which agrees with the higher number of taxa of reef-associated fish larvae identified in the southern stations (DWDE-2, Supporting Information Table S1). The propagules could originate in reefs located

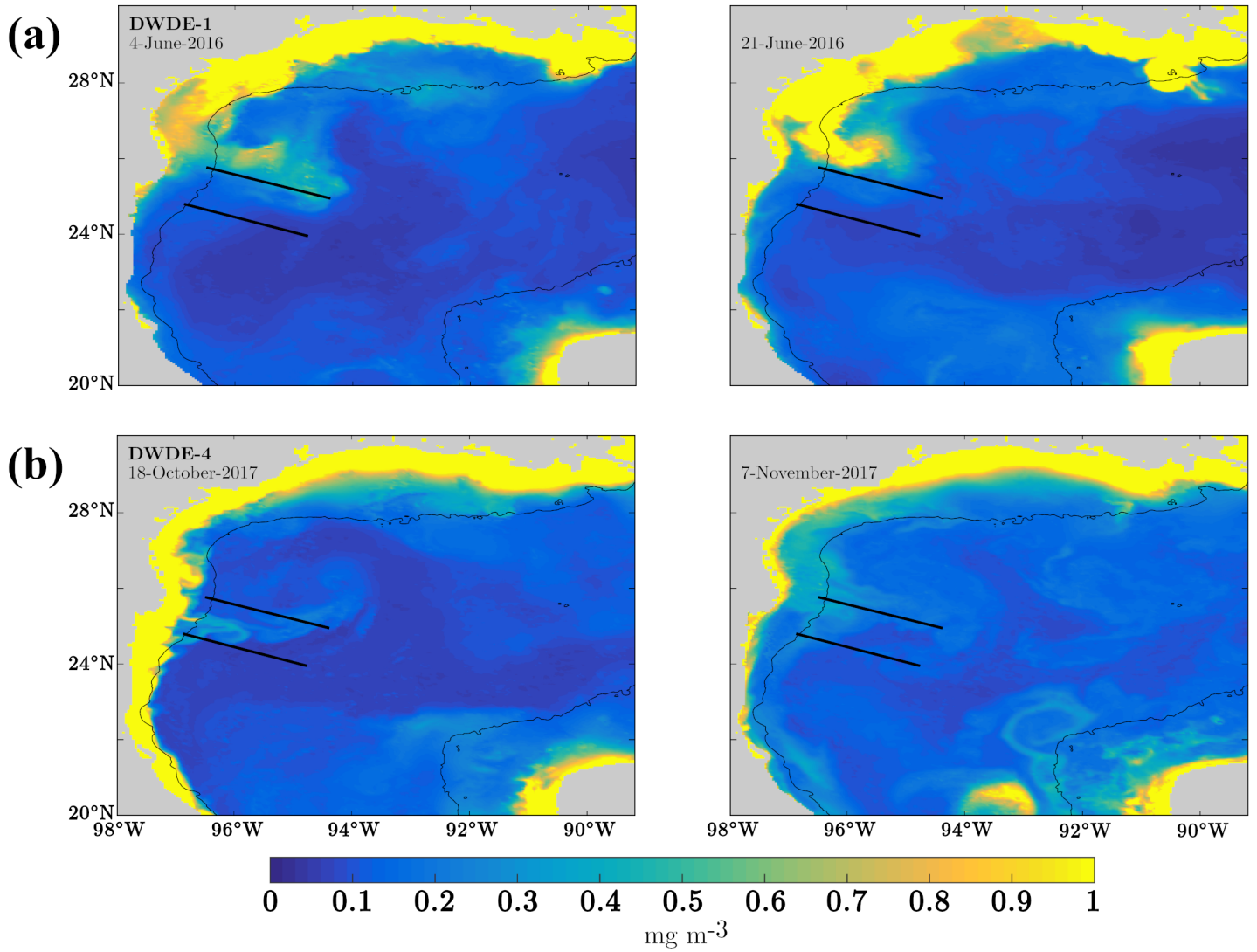

Fig. 7. Surface Chl *a* concentration (mg m^{-3}) obtained from remote sensing data on the date that Chl *a* filaments showed the highest flow into deep waters of the 28 d period preceding each cruise (left), and at the beginning for each them (right): (**a**) DWDE-1 (June 2016), (**b**) DWDE-4 (November 2017), (**c**) DWDE-2 (October 2016), and (**d**) DWDE-3 (April 2017). Black parallel lines indicate the north and south transect positions (the specific location of each station is shown in Fig. 3). The isobath of 200 m is depicted with black line.

in northern Veracruz, as well as the Yucatan platform and Louisiana. Although the Campeche and Yucatan shelves are located relatively far from the deep-water region of Perdido, as compared to that off Texas and northern Veracruz, the potential for connectivity between these sites has been suggested previously by Zavala-Hidalgo et al. (2003).

The lack of connectivity between the Perdido oceanic stations and provinces with reefs in the third simulation experiment (Fig. 5d) is not in complete agreement with the biological outcome. Although the third cruise showed the lowest contribution of reef-associated taxa, a few fish larvae of these taxa were identified in both transects (DWDE-3, Supporting Information Table S1). These larvae may have been subject to dispersal for longer than 28 d. *Bothus* spp., for example, can extend its PLD and metamorphose when suitable nursery habitat is available (Evseenko 2008). Future studies that include age determination based on otolith daily increment counts would be very useful in defining the appropriate PLD for a given taxa (Zapata and Herrón 2002; Schlaefer et al. 2018). The analysis of otolith geochemistry and stable isotope markers can also be helpful to track the origin of fish larvae (Campana et al. 2000; Fodrie and Herzka 2013).

Limitations to this approach

A limitation of this study is that larval behavior was not incorporated in examining dispersal pathways. However, we

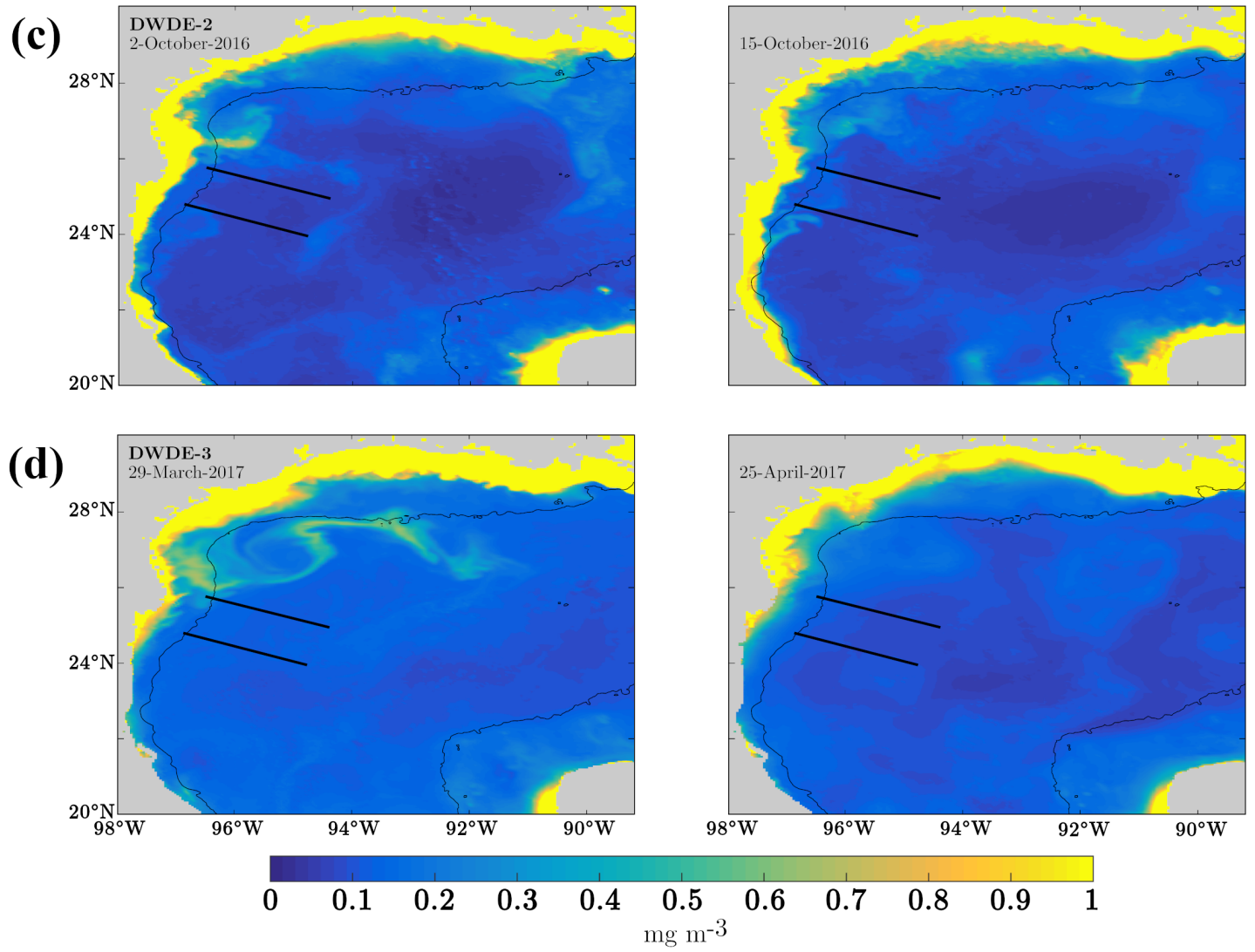

Fig. 7 (Continued)

do account for transport over the top 0–200 m, and therefore the unresolved consequences of ignoring vertical migration have been addressed to some extent by modeling the depths over which diel vertical migration mainly occurs.

We also chose to examine a single PLD (28 d). Endurance swimming abilities are very limited until after notochord flexion is complete (Clark et al. 2005). Since 89.6% of the fish larvae collected were in the preflexion and flexion stages, spawning grounds should not be very far from our sampling regions (Hitchman et al. 2012). Although it is worth considering whether using shorter PLDs would alter our results. Using shorter PLDs (T = 7, 14, or 21 d) to calculate the time-averaged proportions of larvae from coastal and neritic regions resulted in the same general trend: a higher proportion of coastal and neritic larvae was found for DWDE-1 and DWDE-4 than for DWDE-2 and DWDE-3 (Fig. 2). Therefore, the dynamical structures present during the month prior to the cruises were largely responsible of the different larval abundances found offshore.

Last, although fish larvae are moving throughout the upper-layer ocean, larvae from different fish species will have different behaviors. Despite the consistency between biological and numerical results we found, future studies to determine the connectivity of specific species (instead of an ensemble) should contemplate particular traits like vertical migration, mortality, PLD, among others.

Conclusions

Although one must consider that (1) the hourly model output does not resolve fine-scale physical processes that drive

dispersion and hence impact connectivity, and (2) our larval transport model did not include particle behavior, the spatial and temporal resolution of the HYCOM + NCODA version used provided consistent results with the abundances of neritic larvae collected in the in deep-water region of Perdido over 4 weeks. This suggests model simulations with similar resolution can be a useful tool for deriving two-dimensional velocity fields to infer dispersion pathways of planktonic organisms, and can be used for obtaining statistically robust results based on the simulation of a sufficiently large number of Lagrangian particles. Such backtracking experiments will contribute to the understanding of the connectivity levels of continental shelf fish communities with pelagic larvae stages, and are also helpful for identifying the most likely origin of observed propagules, as has been suggested by prior studies (Batchelder 2006; Brickman et al. 2009; Thygesen 2011). This information about larval fluxes will be helpful to interpret the effects of the environment on growth and population dynamics of ichthyoplankton (Batchelder 2006), to predict hatching areas (Christensen et al. 2007), to design marine protected areas (Paris et al. 2009), and to assess the recovery potential to oil spills (Paris et al. 2020).

References

Auditore, P. J., R. G. Lough, and E. A. Broughton. 1994. A review of the comparative development of Atlantic cod (*Gadus morhua* L.) and haddock (*Melanogrammus aeglefinus* L.) based on an illustrated series of larvae and juveniles from Georges Bank. NAFO Sci. Counc. Stud. **20**: 7–18.

Barker, V. A., and J. H. Cowan. 2018. The effect of artificial light on the community structure of reef-associated fishes at oil and gas platforms in the northern Gulf of Mexico. Environ. Biol. Fishes **101**: 153–166. doi:10.1007/s10641-017-0688-9

Batchelder, H. P. 2006. Forward-in-time-/backward-in-time-trajectory (FITT/BITT) modeling of particles and organisms in the coastal ocean. J. Atmos. Ocean. Technol. **23**: 727–741. doi:10.1175/JTECH1874.1

Beldade, R., T. Pedro, and E. J. Gonçalves. 2007. Pelagic larval duration of 10 temperate cryptobenthic fishes. J. Fish Biol. **71**: 376–382. doi:10.1111/j.1095-8649.2007.01491.x

Belkin, I. M., P. C. Cornillon, and K. Sherman. 2009. Fronts in large marine ecosystems. Prog. Oceanogr. **81**: 223–236. doi:10.1016/j.pocean.2009.04.015

Biggs, D., and F. Müller-Karger. 1994. Ship and satellite observations of chlorophyll stocks in interacting cyclone-anticyclone eddy pairs in the western Gulf of Mexico. J. Geophys. Res. **99**: 7371–7384. doi:10.1029/93JC02153

Brickman, D., B. Ådlandsvik, U. Thygesen, C. Parada, K. Rose, A. Hermann, and K. Edwards. 2009. Particle tracking, p. 9–19. *In* North E. W Gallego A and Petitgas P (eds.) Manual of recommended practices for modelling physical-biological interactions in fish early-life history. ICES cooperative research report.

Campana, S. E., G. A. Chouinard, J. M. Hanson, A. Fréchet, and J. Brattey. 2000. Otolith elemental fingerprints as biological tracers of fish stocks. Fish. Res. **46**: 343–357. doi:10.1016/S0165-7836(00)00158-2

Christensen, A., U. Daewel, H. Jensen, H. Mosegaard, M. S. John, and C. Schrum. 2007. Hydrodynamic backtracking of fish larvae by individual-based modelling. Mar. Ecol. Prog. Ser. **347**: 221–232. doi:10.3354/meps06980

Clark, D. L., J. M. Leis, A. C. Hay, and T. Trnski. 2005. Swimming ontogeny of larvae of four temperate marine fishes. Mar. Ecol. Prog. Ser. **292**: 287–300. doi:10.3354/meps292287

CMEMS. n.d. Quality information document. Available from http://marine.copernicus.eu/documents/QUID/CMEMS-OC-QUID-009-030-032-033-037-081-082-083-085-086-098.pdf

CNH. 2019. Comisión Nacional de Hidrocarburos. Recursos Prospectivos de México: Área Perdido, Cordilleras Mexicanas y Cuenca Salina, aguas profundas del Golfo de México. https://www.gob.mx/cms/uploads/attachment/file/527025/Deepwater_Prospective_Resources_of_Mexico_Publishing_2019_DGEPP_low.pdf

Cowen, R. K., C. B. Paris, and A. Srinivasan. 2006. Scaling of connectivity in marine populations. Science **311**: 522–527. doi:10.1126/science.1122039

Evseenko, S. A. 2008. Distribution and routes of drift migrations in larvae of three species of flatfish *Bothus* (Bothidae) in open waters of the northern Atlantic. J. Ichthyol. **48**: 825–843. doi:10.1134/S0032945208090105

Fahay, M. P. 2007. Early stages of fishes in the Western North Atlantic Ocean. Northwest Atlantic Fisheries Organization.

Felder, D. L., and D. K. Camp. 2009. Gulf of Mexico origin, waters and biota. Biodiversity. V. 1. Texas A&M Univ. Press.

Fisher, R., D. R. Bellwood, and S. D. Job. 2000. Development of swimming abilities in reef fish larvae. Mar. Ecol. Prog. Ser. **202**: 163–173. doi:10.3354/meps202163

Fodrie, F. J., and S. Z. Herzka. 2013. A comparison of otolith geochemistry and stable isotope markers to track fish movement: Describing estuarine ingress by larval and post-larval halibut. Estuaries Coast. **36**: 906–917. doi:10.1007/s12237-013-9612-5

Froese, R., and D. Pauly [eds]. 2019. FishBase. World Wide Web electronic publication. version (12/2019) [accessed 2020 November 30]. Available from www.fishbase.org

Fuiman, L. A. 2002. Special considerations of fish eggs and larvae, p. 1–32.*In* L. A. Fuiman and R. G. Werner [eds.], Fishery science: The unique contributions of early life stages. Blackwell Science.

Gough, M. K., F. J. Beron-Vera, M. J. Olascoaga, J. Sheinbaum, J. Jouanno, and R. Duran. 2019. Persistent Lagrangian transport patterns in the northwestern Gulf of Mexico.

J. Phys. Oceanogr. **49**: 353–367. doi:10.1175/jpo-d-17-0207.1

Hamilton, P., Bower, A., Furey, H., Leben, R., and Pérez-Brunius, P. 2016. Deep circulation in the Gulf of Mexico: A Lagrangian study. OCS Study BOEM: 2016-081, 289 pp. https://www.boem.gov/newsroom/lagrangian-study-deep-circulation-gulf-mexico

Hitchman, S. M., N. B. Reyns, and A. R. Thompson. 2012. Larvae define spawning habitat of bocaccio rockfish *Sebastes paucispinis* within and around a large Southern California marine reserve. Mar. Ecol. Prog. Ser. **465**: 227–242. doi:10.3354/meps09926

Houde, E. D. 1989. Comparative growth, mortality, and energetics of marine fish larvae: Temperature and implied latitudinal effects. Fish. Bull. **87**: 471–495.

Irisson, J. O., J. M. Leis, C. B. Paris, and H. I. Browman. 2009. Behaviour and settlement, p. 42–59. *In* North E. W Gallego A and Petitgas P (eds.) Manual of recommended practices for modelling physical-biological interactions during fish early life. International Council for the Exploration of the Sea (ICES).

Jellyman, D., and K. Tsukamoto. 2005. Swimming depths of offshore migrating longfin eels *Anguilla dieffenbachii*. Mar. Ecol. Prog. Ser. **286**: 261–267. doi:10.3354/meps286261

Johnson D. R., Perry H. M., Lyczkowski-Shultz J. 2013. Connections between Campeche Bank and Red Snapper Populations in the Gulf of Mexico via Modeled Larval Transport. Transactions of the American Fisheries Society **142**: 50–58. http://dx.doi.org/10.1080/00028487.2012.720630

Jones, G. P. 2015. Mission impossible: Unlocking the secrets of coral reef fish dispersal, p. 16–27. *In* C. Mora [ed.], Ecology of fishes on coral reefs. doi:10.1017/CBO9781316105412.004. Cambridge Univ. Press.

Lara-Hernández, J. A., J. Zavala-Hidalgo, L. Sanvicente-Añorve, and P. Briones-Fourzán. 2019. Connectivity and larval dispersal pathways of *Panulirus argus* in the Gulf of Mexico: A numerical study. J. Sea Res. **155**: 101814. doi:10.1016/j.seares.2019.101814

Largier J. L. 2003. Considerations in estimating larval dispersal distances from oceanographic data. Ecological Applications **13**: (sp1) 71–89. http://dx.doi.org/10.1890/1051-0761(2003)013[0071:cieldd]2.0.co;2

Leis, J. M. 2006. Are larvae of demersal fishes plankton or nekton? Adv. Mar. Biol. **51**: 57–141. doi:10.1016/S0065-2881(06)51002-8

Liddell, W. D. 2007. Origin and geology, p. 23–33.*In* J. W. J. Tunnell, E. A. Chávez, and K. Withers [eds.], Coral reefs of the southern Gulf of Mexico. Texas A&M Univ. Press.

Macpherson, E., and N. Raventos. 2006. Relationship between pelagic larval duration and geographic distribution of Mediterranean littoral fishes. Mar. Ecol. Prog. Ser. **327**: 257–265. doi:10.3354/meps327257

Majoris, J. E., K. A. Catalano, D. Scolaro, J. Atema, and P. M. Buston. 2019. Ontogeny of larval swimming abilities in three species of coral reef fishes and a hypothesis for their impact on the spatial scale of dispersal. Mar. Biol. **166**: 1–14. doi:10.1007/s00227-019-3605-2

Martínez-López, B., and J. Zavala-Hidalgo. 2009. Seasonal and interannual variability of cross-shelf transports of chlorophyll in the Gulf of Mexico. J. Mar. Syst. **77**: 1–20. doi:10.1016/j.jmarsys.2008.10.002

Nash, H. L., S. J. Furiness, and J. W. Tunnell Jr. 2013. What is known about species richness and distribution on the outer — shelf South Texas Banks? Gulf Caribb. Res. **25**: 9–18. doi:10.18785/gcr.2501.02

National Oceanic and Atmospheric Administration (NOAA). 2020. Historical hurricane tracks. NOAA Office for Coastal Management. Website last modified on June 28, 2018 [accessed 2020 January]. Available from https://coast.noaa.gov/hurricanes/

Olascoaga, M. J., I. I. Rypina, M. G. Brown, F. J. Beron-Vera, H. Koçak, L. E. Brand, G. R. Halliwell, and L. K. Shay. 2006. Persistent transport barrier on the West Florida Shelf. Geophys. Res. Lett. **33**: 1–5. doi:10.1029/2006GL027800

Paris, C. B., R. K. Cowen, K. M. M. Lwiza, D. P. Wang, and D. B. Olson. 2002. Multivariate objective analysis of the coastal circulation of Barbados, West Indies: Implication for larval transport. Deep-Sea Res. I Oceanogr. Res. Pap. **49**: 1363–1386. doi:10.1016/S0967-0637(02)00033-X

Paris, C. B., and R. K. Cowen. 2004. Direct evidence of a biophysical retention mechanism for coral reef fish larvae. Limnol. Oceanogr. **49**: 1964–1979. doi:10.4319/lo.2004.49.6.1964

Paris, C. B., L. M. Chérubin, and R. K. Cowen. 2007. Surfing, spinning, or diving from reef to reef: Effects on population connectivity. Mar. Ecol. Prog. Ser. **347**: 285–300. doi:10.3354/meps06985

Paris, C. B., J. O. Irisson, G. Lacroix, Ø. Fiksen, J. M. Leis, and C. Mullon. 2009. Application 2: Connectivity, p. 63–76. *In* North E. W Gallego A and Petitgas P. Manual of recommended practices for modelling physical-biological interactions in fish early-life history. ICES cooperative research report.

Paris, C. B., S. A. Murawski, M. J. Olascoaga, A. C. Vaz, I. Berenshtein, P. Miron, and F. J. Beron-Vera. 2020. Connectivity of the Gulf of Mexico continental shelf fish populations and implications of simulated oil spills, p. 369–389.*In* S. A. Murawski, C. H. Ainsworth, S. Gilbert, D. J. Hollander, C. B. Paris, M. Schlüter, and D. L. Wetzel [eds.], Scenarios and responses to future deep oil spills: Fighting the next war. doi:10.1007/978-3-030-12963-7_22. Springer International Publishing.

Pepin, P. 2002. Population analysis, p. 112–142.*In* L. A. Fuiman and R. G. Werner [eds.], Fishery science: The unique contributions of early life stages. Blackwell Science.

Pérez-Brunius, P., P. García-Carrillo, J. Dubranna, J. Sheinbaum, and J. Candela. 2013. Direct observations of the upper layer circulation in the southern Gulf of Mexico. Deep-Sea Res. II Top. Stud. Oceanogr. **85**: 182–194. doi:10.1016/j.dsr2.2012.07.020

Puebla, O., E. Bermingham, and W. O. McMillan. 2012. On the spatial scale of dispersal in coral reef fishes. Mol. Ecol. **21**: 5675–5688. doi:10.1111/j.1365-294X.2012.05734.x

Richards, W. J. [ed.]. 2005. Early stages of Atlantic fishes: An identification guide for the Western Central North Atlantic. V. 1 and 2. CRC Press.

Rooker, J. R., A. M. Landry, B. W. Geary, and J. A. Harper. 2004. Assessment of a shell bank and associated substrates as nursery habitat of postsettlement red snapper. Estuar. Coast. Shelf Sci. **59**: 653–661. doi:10.1016/j.ecss.2003.11.009

Sale, P. F. 1991. The ecology of fishes on coral reefs. doi:10.1016/C2009-0-02443-X. Academic Press.

Sammarco, P. W. 2014. Determining the geographical distribution, and genetic affinities of corals on offshore platforms, Northern Gulf of Mexico. OCS Study publication BOEM 2014-011. Bureau of Ocean Energy Management.

Sanvicente-Añorve, L., J. Zavala-Hidalgo, M. E. Allende-Arandía, and M. Hermoso-Salazar. 2014. Connectivity patterns among coral reef systems in the southern Gulf of Mexico. Mar. Ecol. Prog. Ser. **498**: 27–41. doi:10.3354/meps10631

Schlaefer, J. A., E. Wolanski, J. Lambrechts, and M. J. Kingsford. 2018. Wind conditions on the Great Barrier Reef influenced the recruitment of snapper (*Lutjanus carponotatus*). Front. Mar. Sci. **5**: 1–20. doi:10.3389/fmars.2018.00193

Siegel, D. A., B. P. Kinlan, B. Gaylord, and S. D. Gaines. 2003. Lagrangian descriptions of marine larval dispersion. Mar. Ecol. Prog. Ser. **260**: 83–96. doi:10.3354/meps260083

Sponaugle, S., and others. 2002. Predicting self-recruitment in marine populations: Biophysical correlates and mechanisms. Bull. Mar. Sci. **70**: 341–375. https://escholarship.org/uc/item/0fk577vf

Sturges, W. 1993. The annual cycle of the western boundary current in the Gulf of Mexico. J. Geophys. Res. **98**: 18053. doi:10.1029/93JC01730

Thygesen, U. H. 2011. How to reverse time in stochastic particle tracking models. J. Mar. Syst. **88**: 159–168. doi:10.1016/j.jmarsys.2011.03.009

Werner, F. E., R. K. Cowen, and C. B. Paris. 2007. Coupled biological and physical models. Oceanography **20**: 54–69. doi:10.5670/oceanog.2007.29

Zapata, F. A., and P. A. Herrón. 2002. Pelagic larval duration and geographic distribution of tropical eastern Pacific snappers (Pisces: Lutjanidae). Mar. Ecol. Prog. Ser. **230**: 295–300. doi:10.3354/meps230295

Zavala-Hidalgo, J., S. L. Morey, and J. J. O'Brien. 2003. Seasonal circulation on the western shelf of the Gulf of Mexico using a high-resolution numerical model. J. Geophys. Res. **108**: 3389. doi:10.1029/2003JC001879

Acknowledgments

We thank Julio Sheinbaum for the recommendation of using the data assimilated HYCOM model to backtrack the possible origin of the larvae collected during the cruises. María Josefina Olascoaga provided helpful advice as well as code for the particle tracking experiments. JLab was used for coordinate transformation in the calculations (http://www.jmlilly.net/software). We are grateful to the crew of the R/V *Pelican* for their professional and willing support during the DWDE cruises, as well as the hard work and cheerful disposition of the scientific crew working with us at sea. The HYCOM + NCODA model outputs were provided by the HYCOM Consortium for Data Assimilative Modeling via their webpage https://www.hycom.org/data/goml0pt04/expt-32pt5. Jesus C. Compaire is grateful to CONICET (Consejo Nacional de Investigaciones Científicas y Técnicas) from Argentina for financial support during the manuscript preparation. This research has been funded by the Mexican National Council for Science and Technology—Mexican Ministry of Energy—Hydrocarbon Fund, project 201441. This is a contribution of the Gulf of Mexico Research Consortium (CIGoM). We acknowledge PEMEX's specific request to the Hydrocarbon Fund to address the environmental effects of oil spills in the Gulf of Mexico. This study has been conducted using E.U. Copernicus Marine Service Information http://marine.copernicus.eu/. We appreciate the comments and suggestions from three anonymous reviewers that helped to significantly improve this manuscript.

Conflict of Interest

None declared.

Submitted 07 April 2020
Revised 17 December 2020
Accepted 17 March 2021

Associate editor: Thomas Kiørboe